Surface & Coatings Technology 205 (2011) 5387–5393

Contents lists available at ScienceDirect

Surface & Coatings Technology

journal homepage: www.elsevier.com/locate/surfcoat

Functional silica film on stainless steel mesh with tunable wettability

Hao Yang [a,b], Xingjuan Zhang [a], Zhi-Qi Cai [a], Pihui Pi [a], Dafeng Zheng [a], Xiufang Wen [a], Jiang Cheng [a], Zhuo-ru Yang [a,*]

[a] School of Chemistry and Chemical Engineering, South China University of Technology, Wushan Road, Guangzhou, 510640, PR China
[b] Key Laboratory for Green Chemical Process of Ministry of Education and School of Chemical Engineering and Pharmacy, Wuhan Institute of Technology, Xiongchu Street, Wuhan, 430073, PR China

ARTICLE INFO

Article history:
Received 5 January 2011
Accepted in revised form 31 May 2011
Available online 12 June 2011

Keywords:
Superhydrophobicity
Superoleophilicity
Superamphiphilicity
Amphiphobicity
Sol–gel process
Oil/water separation

ABSTRACT

A series of functional silica films on stainless steel meshes are fabricated by simple sol–gel process using tetraethyl orthosilicate (TEOS) and methyltriethoxysilane (MTES) as precursors and post-thermal treatment or hydrophobization. The wettabilities of these meshes can range from superhydrophobicity and superoleophilicity to superamphiphilicity or amphiphobicity. The tunable wetting states are controlled by changing surface chemistry or morphology. Firstly, methyl-endcapped silica film with superhydrophobic and superoleophilic property is formed using a dip-coating method; then, the methyl groups are removed by adequate annealing, and the mesh exhibits superamphiphilic property; finally, after surface modification by perfluorooctyltriethoxysilane, the amphiphobic mesh is obtained. These stainless steel meshes with different wettabilities may act as "smart" switches, which can allow oil or water pass through the mesh or not selectively, and this is potential to be used in intelligent oil/water separating device.

1. Introduction

In recent years, the wettability of solid surface has attracted great interests both in academic research [1–4] and practical applications [5–8], particularly for the special wetting behaviors, such as superhydrophobicity [9–11], superhydrophilicity [12–14], superoleophobicity [15–17] and superoleophilicity [18,19]. Materials combining any two different wetting behaviors of solid surface have many potential applications for their functional properties. For example, superhydrophobic and superoleophobic surfaces (also called superamphiphobic surfaces) of textiles have self-cleaning properties by means of repelling oils and water [20,21]; superhydrophilic and superoleophilic surfaces (also called superamphiphilic surfaces) of windshield glasses can keep transparent and clean when liquids contact on the windshield [22,23]. And superhydrophobic and superoleophilic (abbreviated as Shy-Sol) surfaces of filters can separate water from oil (or oil from water) easily and efficiently due to the interfacial phenomena [24–26].

Furthermore, different wetting states can be switched from each other, which were proved to be feasible and potentially useful in industrial, environmental, and biological applications, such as microfluidics, drug-delivery, biosensor and protein enrichment [27–30]. The tunable wettability of surface can be realized by various methods, including light-irradiation [31,32], use of an electric field [33,34], thermal treatment [35,36] and treatment with solvents [37,38]. For instance, surfaces with harshly rough nanostructures modified with fluorinated monolayer or long chain of fatty acids can be turned from superhydrophobicity to superhydrophilicity by exposing to ultraviolet light [39,40]. Thermoresponsive amphiphilic copolymers surfaces with roughness can be swithed from superhydrophilicity to superhydrophobicity with increasing temperature due to the hydrogen bonds variation [41,42]. This inspires the possibilities of transitions among superamphiphobicity, superamphiphilicity and superhydrophobicity and superoleophilicity.

In this paper, tunable wettabilities of stainless steel meshes were obtained as follows: firstly, a Shy-Sol silica film was fabricated on stainless steel mesh using sol–gel process, and the mesh can separate water from oil easily. The efficiency for oil/water separation can be found in Supplementary Data. Secondly, the mesh was treated with elevated temperature and the wettability of the mesh was switched from superhydrophobicity to superhydrophilicity while maintaining superoleophilicity. It allowed both oil and water pass through the mesh. At last, self-assembled monolayer of perfluorooctyltriethoxysilane was coated on the thermal treated mesh, the obtained mesh exhibited amphiphobic property, and oil and water were prevented to pass through the mesh. Schematic illustration of different oil/water separating states of stainless steel meshes with different wetting properties can be seen in Fig. 1. The tunable wetting meshes can thus be used as switches to control oil or water penetrating the mesh and may have potential application in smart oil/water separating device.

* Corresponding author at: School of Chemistry and Chemical Engineering, South China University of Technology, Wushan RD., Tianhe District, Guangzhou, Guangdong, 510640, PR China. Tel.: +86 20 87112057 801; fax: +86 20 87112057 804.
E-mail address: Zhryang@scut.edu.cn (Z. Yang).

0257-8972/$ – see front matter © 2011 Elsevier B.V. All rights reserved.
doi:10.1016/j.surfcoat.2011.05.049

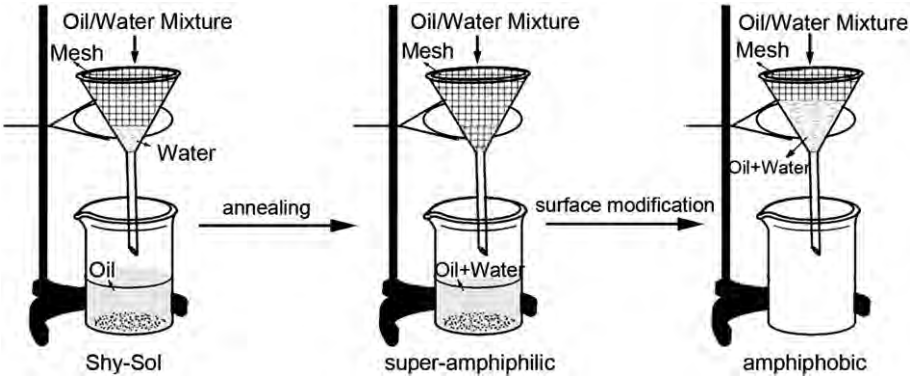

Fig. 1. Schematic illustration of different oil/water separating states on stainless steel meshes with different wetting properties.

2. Material and methods

2.1. Preparation of silica sol

The preparation of hydrophobic silica sol was carried out using a method described in our previous work [43]. Briefly, 7 mL (0.03 mol) tetraethyl orthosilicate (TEOS, 98%, analytical reagent, abbreviated as A. R.) was added to 5 mL (0.13 mol) ammonia (NH_3, 25% in water, A.R.), 9 mL (0.5 mol) deionized water (H_2O) and 100 mL (1.74 mol) absolute ethanol (EtOH, 99.5%, A.R.) under rapid stirring using a mechanical agitator. The mixture was allowed to react at 60 °C for 90 min. Then, 3.9 mL (0.02 mol) methyltriethoxysilane (MTES, 98%, A.R.) was added dropwise to the mixture and stirred for 19 h to avoid gel formation. As a result, the silica sol cannot turn to gel within one week, which can prolong the service life of the sol solution. The obtained silica sol was composed of about 220 nm spheric silica nanoparticles, and the polydispersity index of the nanoparticles was 0.028, which indicated that the silica sol was monodisperse and stable (see Fig. S1).

2.2. Preparation of samples

The procedure for preparing different wetting properties of stainless steel meshes is outlined in Fig. 2. Shy-Sol silica film on stainless steel mesh was prepared based on a dip-coating method described earlier [43]. In detail, fresh silica sol solutions were aged for 3 days at ambient temperature and pressure, and then stainless steel mesh was dipped into the sol solutions for about 5 min, and dried at 110 °C for 30 min. This procedure was recycled 4 times to get enough roughness of the silica film. Shy-Sol mesh was acquired at 400 °C for 2 h. After that, the mesh was annealed at 600 °C for another 2 h to gain superamphiphilic property. Lastly, amphiphobic mesh was obtained by further surface modification using perfluorooctyltriethoxysilane.

Surface modification of the stainless steel mesh was conducted as follows: the mesh was put into the mixtures of perfluorooctyltriethoxysilane (Dynasylan F8261, Degussa), EtOH, H_2O and 0.1 M hydrochloric acid in 0.5/88/10/1.5 weight percentage for 30 min and was dried at 120 °C for 2 h. The resultant mesh was washed in ethanol under ultrasonication to remove surplus silica and dried prior to analysis.

2.3. Characterization

The surface morphology of the silica film was measured by field-emission scanning electron microscopy (FESEM, LEO 1530 VP, Germany). The surface roughness of the film was characterized by atomic force microscope (AFM, CSPM5000, Benyuan, China). Scanning scope is 25 × 25 μm. The surface chemical composition of the film was

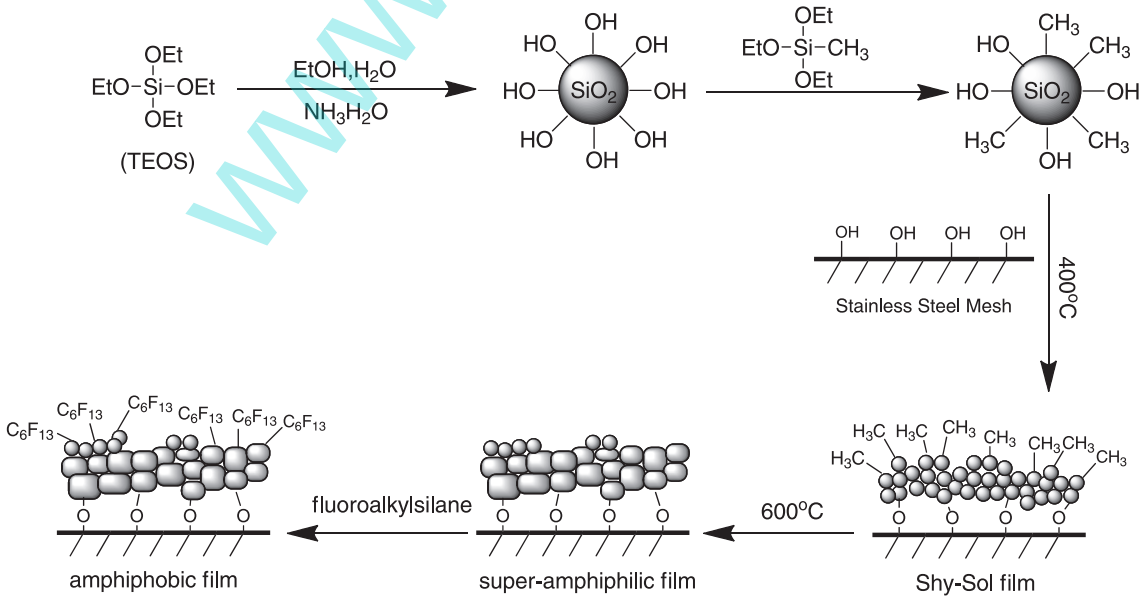

Fig. 2. Schematic diagram of procedure to fabricate Sho-Sol, superamphiphilic and amphiphobic silica films on stainless steel meshes.

determined by X-ray photoelectron spectroscopy (XPS). XPS data were collected in both survey and high-resolution mode on Kratos Axis Ultra DLD systems equipped with Al Kα X-ray source and operating at 300 W. Elementary analyzer (Vario EL III, Elementary, Germany) was used to calculate quantitatively the organic content of the silica nanoparticles. The decomposition temperature of the organic groups of the nanoparticles was computed by thermogravimetric analyses and differential scanning calorimetry (TG-DSC, NETZSCH STA449C, Germany) by heating the sample (8 mg) in a flow of air (30 mL/min) at 10 °C/min from room temperature to 1000 °C. The samples for TG-DSC were prepared by evaporating 10 mL of the colloidal suspension under ambient conditions for several hours till powders of constant weight were obtained.

Static contact angle and tilt angle measurements were performed with an optical contact angle meter (OCA40 Micro, Dataphysics, Germany). The wettability of the stainless steel meshes was determined by measuring the contact angles of three probe liquids, water ($\gamma = 72.8$mN/m), aviation kerosene ($\gamma = 22$–26 mN/m) and diiodomethane ($\gamma = 50.8$ mN/m). The hydrophobicity and oleophilicity were measured respectively with 5 μL water and 5 μL diiodomethane or aviation kerosene. An average of five measurements was made to determine the hydrophobicity and oleophilicity of the film. The tilt angles were measured by immobilizing the meshes on a plate and tilting both the microscope and the plate until 5 μL water droplet rolling off the meshes.

3. Results and discussions

3.1. Shy-Sol mesh

Silica nanoparticles are usually hydrophilic or even superhydrophilic when prepared by well-known Stöber method since the surface of the particles is fully covered with silanol groups (Si–OH) [44,45]. In order to get hydrophobic silica nanoparticles, MTES is usually used as hydrophobic reagent to graft methyl groups on the surface of the silica nanoparticles [46–48]. MTES can hydrolyze ethyoxyl groups to generate silanol groups, which can react with silanol groups of the silica nanoparticles produced by sol–gel process using TEOS, finally introducing Si–CH_3 groups on the silica nanoparticles. The reaction mechanism can be found in references [43,49]. The remaining silanol groups of the silica nanoparticles can condense with the hydroxyl groups of the stainless steel mesh to make the silica nanoparticles adhere to the mesh.

The Shy-Sol silica film can be formed on the stainless steel mesh using simple dip-coating method and post thermal treatment as seen in Fig. 2. The thermal treatment was under conditions of 400 °C for 2 h. The wettability of the Shy-Sol mesh is investigated by water and aviation kerosene. The results show that the water contact angle (WCA) of the mesh is 154.8°, and water tilt angle (WTA) is 9.2° (Fig. 3(a)), which shows superhydrophobicity. And 5 μL aviation kerosene droplet can spread out on the mesh in less than 160 ms (Fig. 3(b)), which proves superoleophilicity. Besides, the wettability of the mesh is nearly unchangeable after pouring with 2 kg/cm^2 water stream, which indicates good adherency of the silica film on stainless steel mesh. This special wetting phenomenon can be attributed to the synergy effects of surface chemistry and morphology.

The hydrophobicity of the silica film is obtained by eliminating of the silanol groups of the silica nanoparticles and shielding of other residual silanol groups [50]. However, WCA of a pure homogeneous and ideally smooth surface with CH_3-terminated domains is only 110.0° [51,52], which is much smaller than the WCA of the mesh obtained in our experiment. So it can be deduced that the hydrophobicity is enhanced intensely by the special surface structure of the silica film. The surface morphology of the mesh can be observed by FESEM, shown in Fig. 4 (a)–(d). From these images, it can be seen that the smooth stainless steel wires are completely coated by the silica film. The thickness of the film is less than 6 μm (see Fig. S2) and has little effect on the pore size of the mesh (75 μm), which is a very important parameter for oil/water

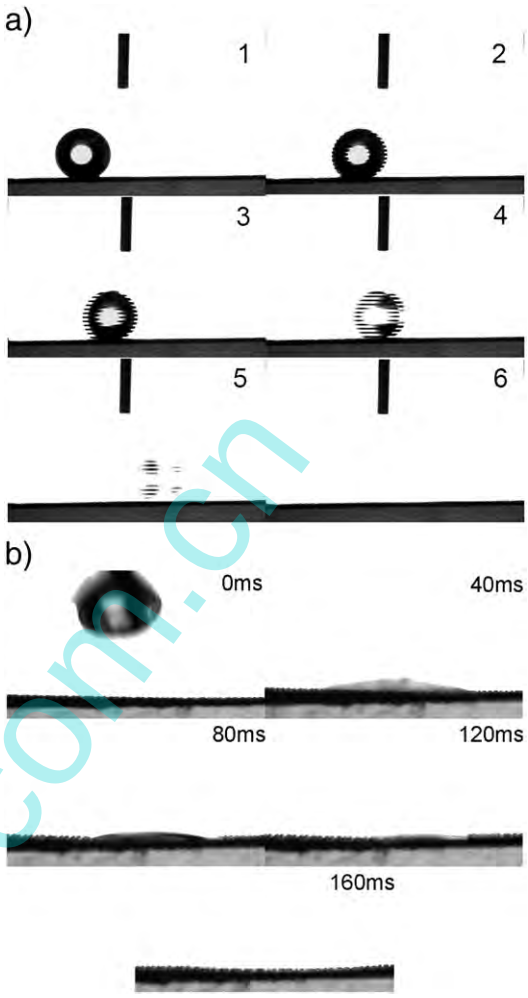

Fig. 3. (a) Images of 5 μL water droplet rolling off the silica film(The WTA is 9.2°); (b) Images of 5 μL aviation kerosene droplet spreading out on the silica film.

separation. The silica film consists of sphere silica nanoparticles with the diameter of about 220 nm. And it also can be found in Fig. 4 that irregular clusters with the average sizes of 1–5 μm are formed by aggregating hundreds of silica nanoparticles. Thus the micro-nano-binary structure is constructed on the mesh as the lotus leaf. Indeed, considering the structures of the stainless steel mesh with 45 μm diameters of wires and 75 μm of pore size, there are three levels of roughness on our samples.

The relationship between contact angle and surface roughness can be well described by the Cassie–Baxter equation [53].

$$\cos\theta r = f_1 \cos\theta - f_2 \quad (1)$$

Where θ_r and θ are contact angles of rough and flat surfaces, respectively; f_1 and f_2 are the corresponding fractions of the solid surface and air in contact with the liquid, $f_1 + f_2 = 1$. This equation indicates that the larger air fraction (f_2), the more hydrophobic of the surface. In our experiment, θ_r and θ are 154.8° and 110.0°, respectively, both nanoscale sphere silica particles structure and microscale irregular clusters structure can bring a large quantity of trapped air when in contact with water ($f_2 = 0.855$, calculated based on Eq. (1)), which is essential for the mesh to show superhydrophobicity.

On the other hand, surface with CH_3-terminated domains is intrinsically oleophilic because of the similarity in chemical component. When oil drop contacts with the silica film, the oil is drawn into the air pocket. In the other words, air is replaced by the oil. Moreover, the

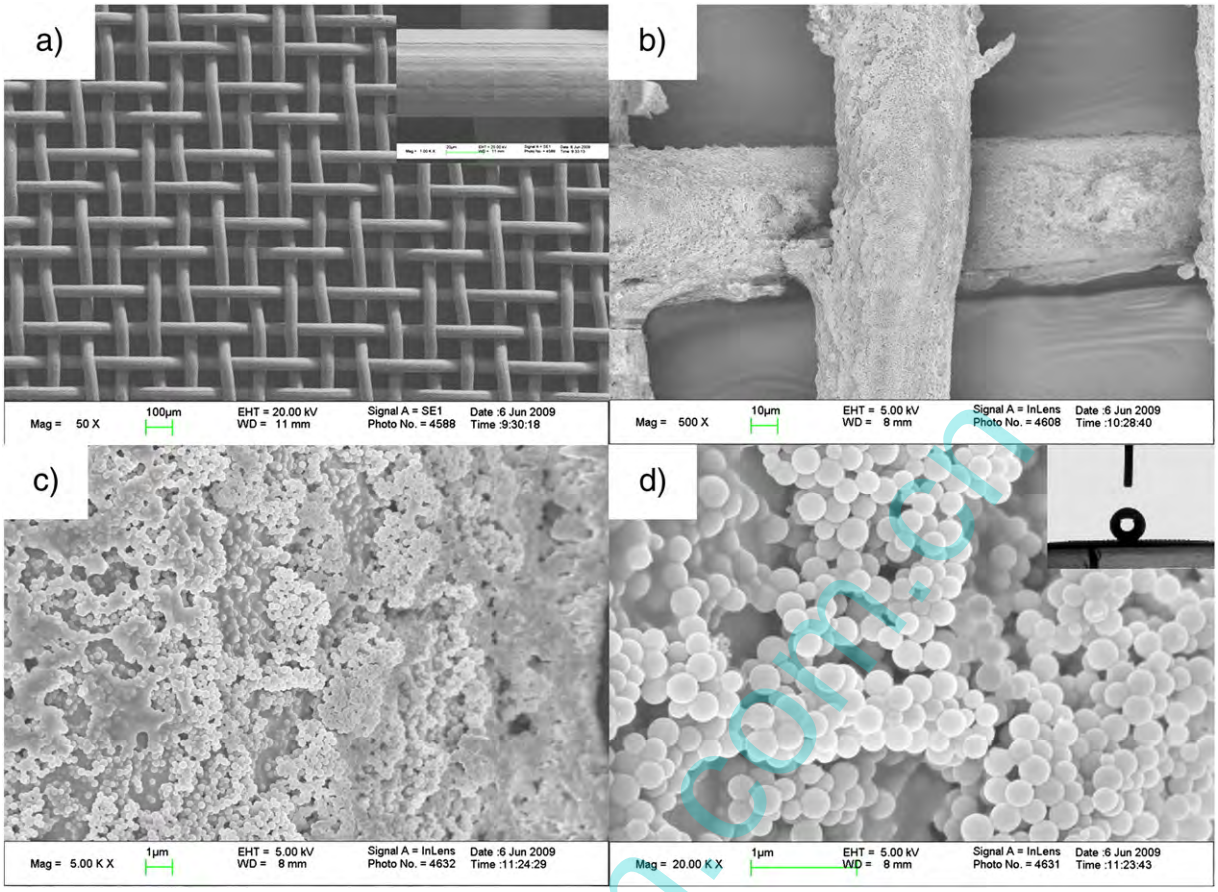

Fig. 4. FESEM images of the pristine stainless steel mesh and Shy-Sol mesh. (a) stainless steel mesh, the inset is the higher-magnification image. (b), (c), (d) are different magnification images of the Shy-Sol mesh at 500X, 5.0 K X and 20.0 K X respectively. The inset in (d) is the image of a static water droplet (5 μL) on the film.

hollow structure of the porous silica film and the low adhesion between oil and the film make oil penetrate the film. In fact, oil can penetrate the mesh rapidly and completely by means of capillary action [54]. In conclusion, the micro-nano-binary structure of the silica film enhances the wetting of oil and non-wetting of water.

3.2. Superamphiphilic mesh

According to the mechanism of wettability, tailoring the surface structure or controlling the surface coverage of hydrophobic organic groups on the silica framework can change the wettability of the silica film [55–58]. In our experiment, altering the annealing temperature can realize the tunable wettabilities of the silica films on stainless steel meshes. After annealed at 600 °C for 2 h, the WCA of the mesh varies from 154.8° to almost 0°, and the WTA varies from 9° to an immeasurable value, for water droplet spreads out on the mesh too fast to be measured. The relationship between the WCA and WTA of the mesh and its annealing temperature is shown in Fig. 5. It can be seen from Fig. 5 that the WCAs increase slowly and WTAs decrease with the annealing temperature increasing from 110 °C to 400 °C.

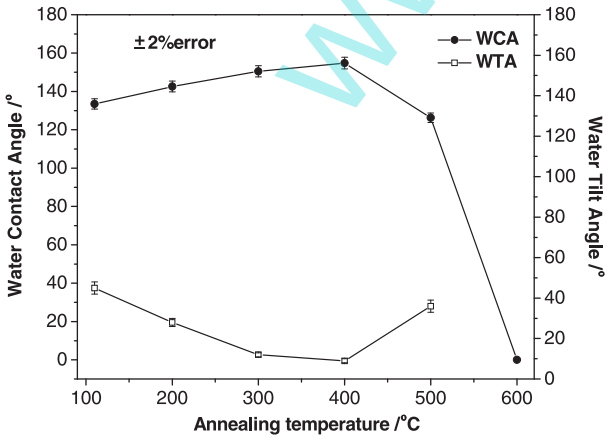

Fig. 5. Relationship between the WCA and WTA of the mesh and its annealing temperature.

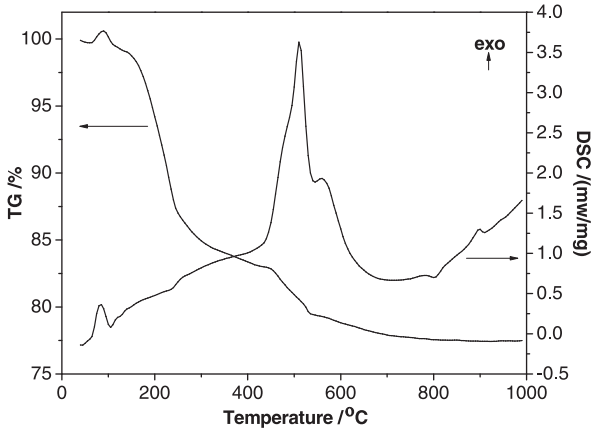

Fig. 6. TG–DSC curves of the as-prepared hydrophobic silica nanoparticles.

Table 1
C and H elements contents of the silica nanoparticles at different annealing temperatures.

Annealing temperature (°C)	C element content (%)	H element content (%)
110	7.743	2.150
200	7.394	2.049
300	5.167	1.745
400	3.943	1.208
500	0.388	0.243
600	0	0

However, if the silica film is annealed above 400 °C, the WCAs decrease sharply and WTAs increase. And at last, the mesh turns to be superhydrophilic after annealed at 600 °C.

The TG–DSC curves shown in Fig. 6 reveal the change of surface chemistry of the silica nanoparticles with increasing temperature. The TG curve gives 20.72% weight loss with respect to the increase in temperature within the range of 110–600 °C, which is much larger than the silica nanoparticles prepared by Stöber method at the same range (4.82%, see Fig. S3). The strong exothermic peak corresponding to the oxidation of surface organic groups (methyl groups) is well resolved in the DSC curve at 511.4 °C. To quantitatively analyze the decomposition ration of the methyl groups, C and H elements contents of the silica nanoparticles at different annealing temperatures are displayed in Table 1. The results indicate that both the C and H elements contents decrease within the range of 110–600 °C, and both of them reach 0 at 600 °C, which suggests that the methyl groups are decomposed completely. Interestingly, the WCAs of the mesh do not decrease owing to the reducing methyl groups below 400 °C. Even when the C element content is only 0.388 at 500 °C, the WCA of the mesh is still as high as 126.3°. Only when annealed at 600 °C, the mesh exhibits superhydrophilicity.

The reason may be resolved in surface roughness. The surface morphologies of the silica film annealed at different temperatures of 110 °C and 600 °C, respectively, are displayed in Fig. 7. It is found that the surface structures of the films are quite different at different temperatures. When annealed at 110 °C, the film is slightly smooth, and the silica nanoparticles are dispersed randomly on the stainless steel wires. The single nanoscale structure is not rough enough to fulfill superhydrophobicity (WCA of the mesh is 133.5°). When raising the temperature, the micro-nano-binary structure is formed (see Fig. 4(d)) and the wetting behavior of the mesh fits Cassie–Baxter regime, so the WCA is affected by the air fraction of the solid surface regardless of the decomposition of methyl groups. Even when the methyl groups are nearly decomposed completely at 500 °C, the film shows water repellency on the hydrophilic surface [59].

However, when annealed at 600 °C, the silica film becomes densification as a transition state of ceramic membrane, which can be seen in Fig. 7(b). The crystal phase transition of the silica nanoparticles is the reason for change of the surface morphology of the silica film, and the XRD patterns of the silica nanoparticles annealed at 110 °C, 400 °C and 600 °C are shown in Fig. S4. Both the micro-nano-binary structure and the porous massive structure coexisting on the silica film indicates that the wetting behavior of the silica film may be the transitional regime between Wenzel's and Cassie's regimes [60], wherein air pocket can be partly replaced by water droplet. Due to the decomposition of the methyl groups of the silica nanoparticles, the hydrophilic film is formed [61,62]. The water droplet is thus absorbed on the film and fills in the air pocket. Owing to the porous structure of the silica film, the hydrophilicity is enhanced and superhydrophilicity is eventually achieved. Besides, the oleophilicity is not affected much by the change of surface chemistry and morphology, because the low surface tension of the aviation kerosene make it prone to wetting the porous structure of the silica film all the time.

3.3. Amphiphobic mesh

The superamphiphilic silica film can further be tuned to be amphiphobic by surface modification with fluoroalkylsilane monolayer without changing the surface morphology. Fluoroalkylsilane is a classic modifying agent to lower surface free energy of materials, because the $-CF_3$ terminated surface is reported to possess the lowest surface free energy [63], about 6mN/m, which is much smaller than the surface tensions of oils, so it is expected to gain the oleophobic property of the film. The WCA and contact angles for diiodomethane and aviation kerosene of the amphiphobic mesh are 145.2°, 126.1° and 117.8°, respectively, and the WTA is slightly large, at about 15–18°. The results reconfirm that the wetting behavior of the silica film annealed at 600 °C is in the transitional regime between Wenzel's and Cassie's regimes, for Cassie's regime has extremely small contact angle hysterisis or WTA, but this value becomes large in the Wenzel one [64].

The surface chemical compositions of the Shy-Sol, superamphiphilic and amphiphobic silica films were determined by XPS analysis. Fig. 8(a) shows that the Shy-Sol film consists of O (37.4%, Atomic

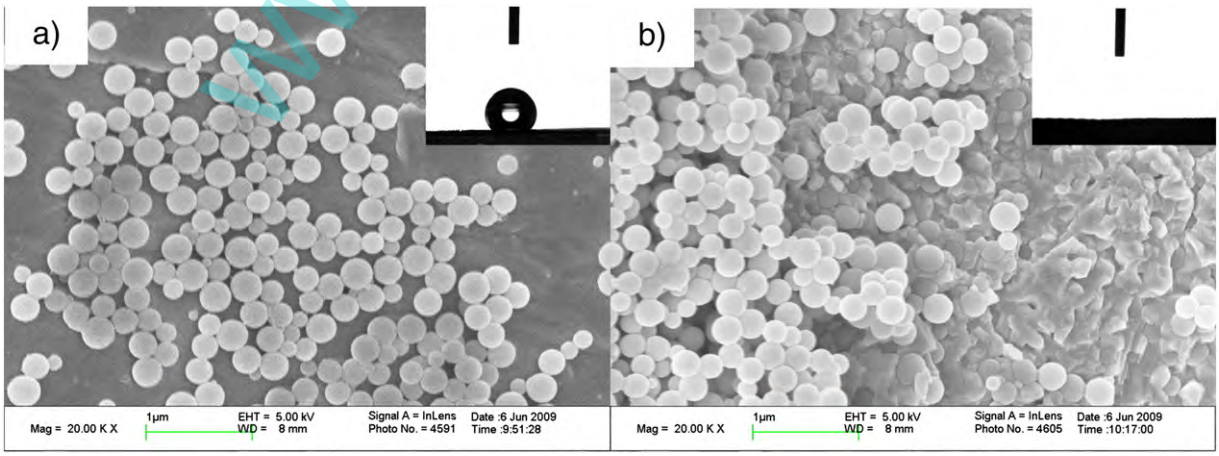

Fig. 7. FESEM images of the silica films annealed at 110 °C(a) and 600 °C(b). The magnification of the images is 20.0 K X. Insets are the images of static water droplets (5 μL) on the meshes.

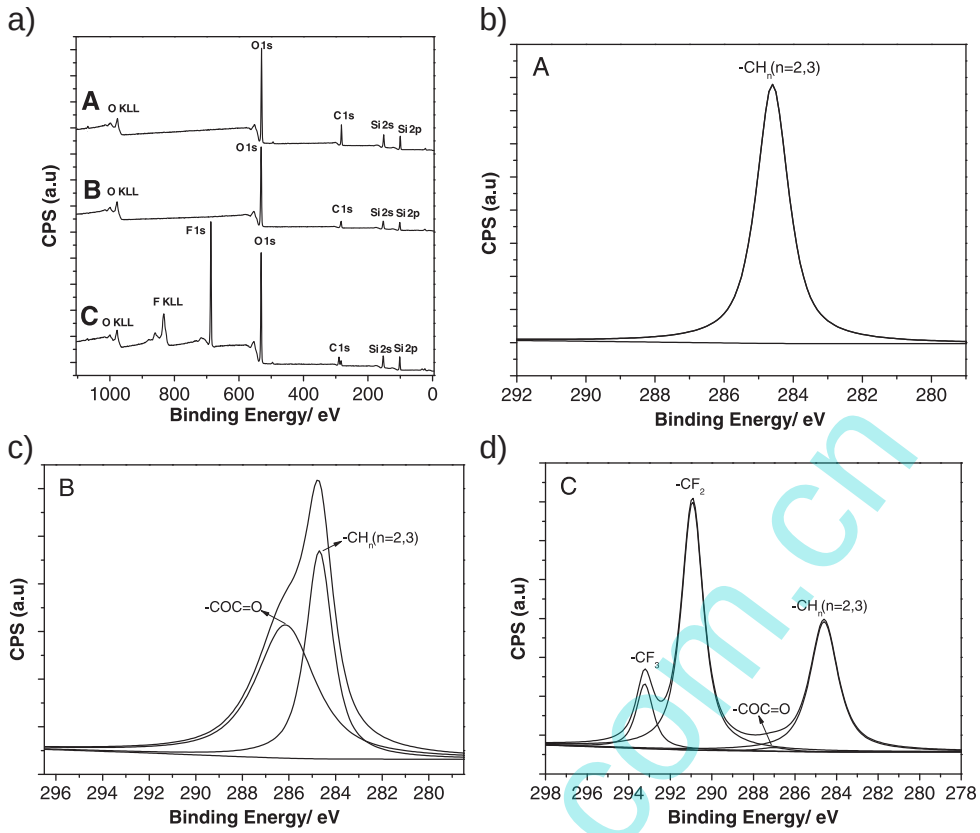

Fig. 8. XPS spectra (a) and C 1 s fitting spectra (b, c, d) of the as-prepared silica films. A, B and C represent Shy-Sol film, superamphiphilic film and amphiphobic film, respectively.

concentration, abbreviated as At%), C(29.3%) and Si(33.3%); superamphiphilic film consists of O(57.5%), Si(26.3%) and C(16.2%); and amphiphobic film consists of O(32.6%), F(24.9%), Si(24.8%) and C (17.7%). C element denotes $-CH_3$ or $-CH_2$, Si element denotes $-SiO$ and F element denotes $-CF_3$ or $-CF_2$ groups. As for O element, it may come from $-SiO$ or oxide of $-CH_3$ at 600 °C, so to clarify the exact groups of the superficial chemical component, the high resolution XPS C 1 s spectra were detected as shown in Fig. 8(b). The Shy-Sol film has only one peak at 284.6 eV, which shows the surface has hydrophobic $-CH_3$; the superamphiphilic film has another peak at 286.1 eV, which may represent $-COC=O$. The area rations for $-COC=O$ and $-CH_3$ are 58.6% and 41.4% respectively, for a large quantity of methyl groups are oxidized compared to Shy-Sol film. The binding energies of 293.2, 290.9, 287.0 and 284.6 eV emerging in amphiphobic film are typical for $-CF_3$, $-CF_2$, $-COC=O$ and $-CH_n$ ($n=2, 3$) moieties, and their area rations are 11.3%, 46.6%, 9.0% and 33.1% respectively. The sum of area for fluorinated groups is as high as 57.9%, and hydrophilic group of $-COC=O$ is sharply reduced from 58.6% to 9%, The results are consistent with TG and elements analyses.

The surface roughness of the Shy-Sol and amphiphobic silica films was investigated by AFM analysis. From the 3D AFM images as shown in Fig. 9, it is found that the surface roughness decreases when the silica film is annealed at 600 °C. Root mean squares (Rms) of the Shy-Sol film and the amphiphobic film are 188 nm and 122 nm, respectively. Fig. 9(a) shows the small mastoid and the hillock-like structure with the relevant WCA (154.8°) and the low WTA (9°), which suggests the Cassie–Baxter regime with air entrapped below the water. Fig. 9(b) presents discontinuous structure with both roughness and flat. The WCA of this film is 145.2°, and the water droplet does not roll off as readily as the film in Fig. 9(a) does. This indicates the transitional regime between Wenzel's and Cassie's regimes, in which water tends to penetrates into the rough surface cavities. Consequently, the surface morphology plays key role in fabricating superhydrophobic films regardless of the surface chemistry.

4. Conclusions

In this article, we fabricated a Shy-Sol silica film on stainless steel mesh using simple sol–gel process. XPS analysis showed that the surface of the silica film contains methyl groups, which is hydrophobic and oleophilic in nature. And micro-nano-binary structure constructed on the stainless steel wires enhances the wetting of oil and non-wetting of the water. The wettability of the Shy-Sol mesh can be tuned by changing the surface structure and chemistry. When annealed at 600 °C, the mesh switches from Shy-Sol surface to superamphiphilic surface due to the transition from Cassie–Baxter regime to Wenzel regime and the oxidation of the methyl groups. When superamphiphilic mesh is further modified with fluoroalkylsilane monolayer, the mesh shows amphiphobic property because of the decrease of surface free energy. These tunable wetting interfacial materials have promising potential to be used in intelligent oil/water separating device.

Supplementary materials related to this article can be found online at doi: 10.1016/j.surfcoat.2011.05.049.

Acknowledgments

This work was supported by “the Fundamental Research Funds for the Central Universities, SCUT” (granted No.: 2009ZM0288).

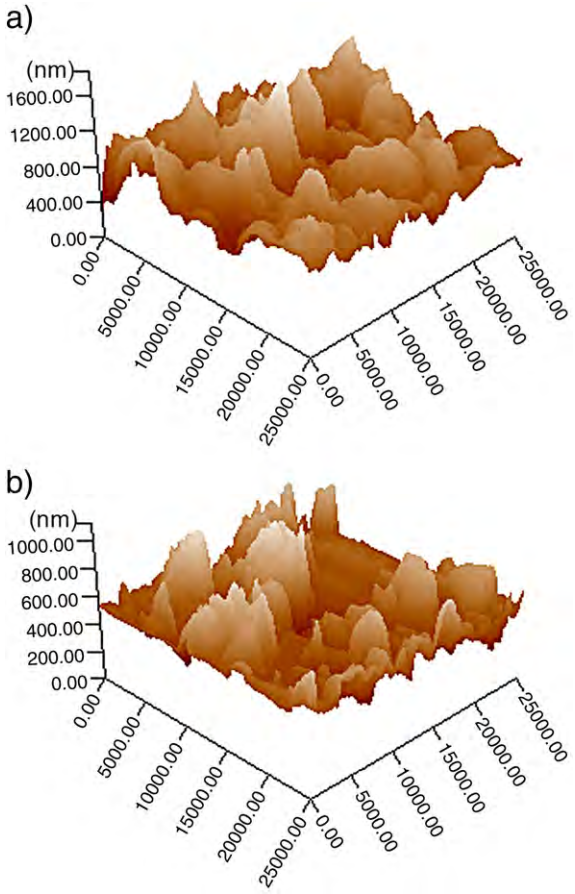

Fig. 9. 3D AFM images of the Shy-Sol film (a) and the amphiphobic film (b).

References

[1] G. Manukyan, J.M. Oh, D. van den Ende, R.G.H. Lammertink, F. Mugele, Phys. Rev. Lett. 106 (2011) 014501.
[2] M.J. Liu, Y.M. Zheng, J. Zhai, L. Jiang, Acc. Chem. Res. 43 (2010) 368.
[3] J.H. Zhang, X.L. Sheng, L. Jiang, Langmuir 25 (2009) 1371.
[4] L.C. Gao, A.Y. Fadeev, T.J. McCarthy, MRS Bull. 33 (2008) 747.
[5] X. Yao, Y.L. Song, L. Jiang, Adv. Mater. 23 (2011) 719.
[6] C. Lee, C.J. Kim, Phys. Rev. Lett. 106 (2011) 014502.
[7] S.A. Kulinich, S. Farhadi, K. Nose, X.W. Du, Langmuir 27 (2011) 25.
[8] Y. Li, L. Li, J.G. Sun, Angew. Chem. Int. Edit. 49 (2010) 6129.
[9] T. Verho, C. Bower, P. Andrew, S. Franssila, O. Ikkala, R.H.A. Ras, Adv. Mater. 23 (2011) 673.
[10] Q.F. Xu, J.N. Wang, K.D. Sanderson, Acs Nano 4 (2010) 2201.
[11] X. Yao, L.A. Xu, L. Jiang, Adv. Funct. Mater. 20 (2010) 3343.
[12] Y.B. Kwon, B.M. Weon, K.H. Won, J.H. Je, Y. Hwu, G. Margaritondo, Langmuir 25 (2009) 1927.
[13] V. Spagnol, H. Cachet, B. Baroux, E. Sutter, J. Phys. Chem. C 113 (2009) 3793.
[14] J.F. Zang, C.M. Li, S.J. Bao, X.Q. Cui, Q.L. Bao, C.Q. Sun, Macromolecules 41 (2008) 7053.
[15] M.J. Liu, S.T. Wang, Z.X. Wei, Y.L. Song, L. Jiang, Adv. Mater. 21 (2009) 665.
[16] B.X. Leng, Z.Z. Shao, G. de With, W.H. Ming, Langmuir 25 (2009) 2456.
[17] L. Joly, T. Biben, Soft Matter 5 (2009) 2549.
[18] T. Darmanin, M. Nicolas, F. Guittard, Langmuir 24 (2008) 9739.
[19] Y.G. Yang, M. Nakazawa, M. Suzuki, H. Shirai, K. Hanabusa, J. Mater. Chem. 17 (2007) 2936.
[20] H.F. Hoefnagels, D. Wu, G. de With, W. Ming, Langmuir 23 (2007) 13158.
[21] A. Tuteja, W. Choi, M.L. Ma, J.M. Mabry, S.A. Mazzella, G.C. Rutledge, G.H. McKinley, R.E. Cohen, Science 318 (2007) 1618.
[22] D. Quere, Ann. Rev. Mater. Res. 38 (2008) 71.
[23] T. Kako, J. Ye, Langmuir 23 (2007) 1924.
[24] S.T. Wang, Y.L. Song, L. Jiang, Nanotechnology 18 (2007) 1.
[25] C.W. Tu, C.H. Tsai, C.F. Wang, S.W. Kuo, F.C. Chang, Macromol. Rapid. Commun. 28 (2007) 2262.
[26] L. Feng, Z.Y. Zhang, Z.H. Mai, Y.M. Ma, B.Q. Liu, L. Jiang, D.B. Zhu, Angew. Chem. Int. Edit. 43 (2004) 2012.
[27] P. Uhlmann, H. Merlitz, J.U. Sommer, M. Stamm, Macromol. Rapid. Commun. 30 (2009) 732.
[28] G.Y. Qing, X. Wang, L. Jiang, H. Fuchs, T.L. Sun, Soft Matter 5 (2009) 2759.
[29] G. Takei, M. Nonogi, A. Hibara, T. Kitamori, H.B. Kim, Lab Chip 7 (2007) 596.
[30] S.T. Wang, H.J. Liu, D.S. Liu, X.Y. Ma, X.H. Fang, L. Jiang, Angew. Chem. Int. Edit. 46 (2007) 3915.
[31] Y.G. Jiang, P.B. Wan, M. Smet, Z.Q. Wang, X. Zhang, Adv. Mater. 20 (2008) 1972.
[32] S.J. Choi, K.Y. Suh, H.H. Lee, J. Am. Chem. Soc. 130 (2008) 6312.
[33] C. Bodre, T. Pauporte, Adv. Mater. 21 (2009) 697.
[34] B. Kakade, R. Mehta, A. Durge, S. Kulkarni, V. Pillai, Nano Lett. 8 (2008) 2693.
[35] H. Yabu, Y. Hirai, M. Kojima, M. Shimomura, Chem. Mater. 21 (2009) 1787.
[36] W. Hou, Q.H. Wang, Langmuir 23 (2007) 9695.
[37] M. Motornov, R. Sheparovych, R. Lupitskyy, E. MacWilliams, S. Minko, Adv. Mater. 20 (2008) 200.
[38] S. Minko, M. Muller, M. Motornov, M. Nitschke, K. Grundke, M. Stamm, J. Am. Chem. Soc. 125 (2003) 3896.
[39] G. Kwak, M. Seol, Y. Tak, K. Yong, J. Phys. Chem. C 113 (2009) 12085.
[40] T.I. Kim, D. Tahk, H.H. Lee, Langmuir 25 (2009) 6576.
[41] J.X. Wang, Y.Q. Wen, J.P. Hu, Y.L. Song, L. Jiang, Adv. Funct. Mater. 17 (2007) 219.
[42] F. Xia, L. Feng, S.T. Wang, T.L. Sun, W.L. Song, W.H. Jiang, L. Jiang, Adv. Mater. 18 (2006) 432.
[43] H. Yang, P.H. Pi, Z.Q. Cai, X.F. Wen, X.B. Wang, J. Cheng, Z.R. Yang, Appl. Surf. Sci. 256 (2010) 4095.
[44] X.M. Liu, J.H. He, J. Phys. Chem. C 113 (2009) 148.
[45] S. Ganjoo, R. Azimirad, O. Akhavan, A.Z. Moshfegh, J. Phys. D. Appl. Phys. 42 (2009) 1.
[46] A.V. Rao, S.S. Latthe, S.A. Mahadik, C. Kappenstein, Appl. Surf. Sci. 257 (2011) 5772.
[47] S.S. Latthe, H. Imai, V. Ganesan, A.V. Rao, Micropor. Mesopor. Mat. 130 (2010) 115.
[48] S.S. Latthe, S.L. Dhere, C. Kappenstein, H. Imai, V. Ganesan, A.V. Rao, P.B. Wagh, S.C. Gupta, Appl. Surf. Sci. 256 (2010) 3259.
[49] Y. Xu, R. Liu, D. Wu, Y. Sun, H. Gao, H. Yuan, F. Deng, J. Non-cryst. Solids. 351 (2005) 2403.
[50] N. Garcia, E. Benito, J. Guzman, P. Tiemblo, J. Am. Chem. Soc. 129 (2007) 5052.
[51] A.M. Almanza-Workman, S. Raghavan, S. Petrovic, B. Gogoi, P. Deymier, D.J. Monk, R. Roop, Thin Solid Films 423 (2003) 77.
[52] A.Y. Fadeev, T.J. McCarthy, Langmuir 16 (2000) 7268.
[53] A.B.D. Cassie, S. Baxter, Trans. Faraday Soc. 40 (1944) 546.
[54] J. Lahann, Nat. Nanotechnol. 3 (2008) 320.
[55] A.V. Rao, S.S. Latthe, D.Y. Nadargi, H. Hirashima, V. Ganesan, J. Colloid Interface Sci. 332 (2009) 484.
[56] S.S. Latthe, H. Imai, V. Ganesan, A.V. Rao, Appl. Surf. Sci. 256 (2009) 217.
[57] S.S. Latthe, D.Y. Nadargi, A.V. Rao, Appl. Surf. Sci. 255 (2009) 3600.
[58] D.A. Doshi, P.B. Shah, S. Singh, E.D. Branson, A.P. Malanoski, E.B. Watkins, J. Majewski, F. van Swol, C.J. Brinker, Langmuir 21 (2005) 7805.
[59] C. Dorrer, J. Ruhe, Adv. Mater. 20 (2008) 159.
[60] S. Wang, L. Jiang, Adv. Mater. 19 (2007) 3423.
[61] N.J. Shirtcliffe, G. McHale, M.I. Newton, C.C. Perry, P. Roach, Mater. Chem. Phys. 103 (2007) 112.
[62] N.J. Shirtcliffe, G. McHale, M.I. Newton, C.C. Perry, P. Roach, Chem. Commun. (2005) 3135.
[63] T. Nishino, M. Meguro, K. Nakamae, M. Matsushita, Y. Ueda, Langmuir 15 (1999) 4321.
[64] H.M. Bok, T.Y. Shin, S. Park, Chem. Mater. 20 (2008) 2247.